Strength evolution of ice plume deposit analogs of Enceladus and Europa

M. Choukroun[1], J.L. Molaro[1,2], R. Hodyss[1], E. Marteau[1], P. Backes[1], E.M. Carey[1], W. Dhaouadi[1,3], S. Moreland[1], E.M. Schulson[4]

[1]Jet Propulsion Laboratory, California Institute of Technology, Pasadena, CA.

[2] Planetary Science Institute, Tucson, AZ.

[3] ETH Zürich, Zurich, Switzerland.

[4] Thayer School of Engineering, Dartmouth College, Hanover, NH.

Corresponding author: Mathieu Choukroun (Mathieu.Choukroun@jpl.nasa.gov)

Key Points:

- The cone penetration resistance of fine-grained porous ice held under isothermal conditions increases linearly over time.
- The temperature dependence of the strengthening rate yields an activation energy similar to self-diffusion at the surface of ice grains.
- Plume deposits would remain weak on Enceladus, while they may develop substantial strength within a few million years on Europa.

Index Terms: Physical properties of materials (5460), Ices (5422), Surface materials and properties (5470), Ice (738)

Keywords: sintering, strength, ice, Europa, Enceladus

Abstract (150 words limit)

Enceladus and possibly Europa spew materials from their internal ocean into their exosphere, some of which are deposited back onto the surface of those Ocean Worlds. This setting provides a unique opportunity to seek traces of past or extant life in ice plume deposits on their surfaces. However, the design of lander missions and surface sampling techniques, and the choice of sampling locations rely heavily on strength expectations. Here we present an experimental investigation of the evolution in strength of ice plume deposit analogs at several temperatures, as well as a model that predicts first-order estimates of the strength of evolved ice plume deposits under geologic timescales relevant to Enceladus and Europa. These results suggest that plume deposits remain weak and poorly consolidated on Enceladus, while they may develop substantial strength (comparable to solid ice) within < 100 My on Europa.

Plain Language Summary

Enceladus and Europa are Ocean Worlds; they harbor an internal ocean beneath their ice shells. There is proof that plumes emit ocean materials out of Enceladus, similar to geysers on Earth, and some evidence for similar activity on Europa. Based on the composition of the plumes and the surface, both Enceladus and Europa are the leading outer Solar System candidates for possibly harboring life. Areas where fresh plume materials are deposited would be the best location to search for traces of life on the surface. A major challenge in preparing mission concepts to explore these locations arises from the need to collect samples of the surface ice, while little is known at present about the mechanical properties of the surface. In this study, we prepared icy plume deposit analogs, and let them evolve in the laboratory over extended periods of time to investigate the evolution of their strength. We find that plume deposits are likely to remain loose and exhibit a low strength over geologic timescales under Enceladus' conditions, suggesting they would be relatively easy to sample. Conversely, under Europa's surface conditions, such plume deposits appear likely to develop a substantial strength.

1. Introduction

Ocean Worlds are outer Solar System objects that harbor an internal liquid water ocean beneath their ice shell (Nimmo & Pappalardo, 2016). Enceladus and Europa are viewed as two of the most likely Ocean Worlds to be habitable, and perhaps inhabited. Their internal oceans are likely in direct contact with the silicate interior (Anderson et al., 1998; Sotin & Tobie, 2004; Schubert et al., 2007; Iess et al., 2014), possibly favoring the development of hydrothermal systems (Zolotov & Shock, 2001b; Glein et al., 2008; Zolotov & Kargel, 2009; Sohl et al., 2010; Sekine et al., 2015) similar to those found on Earth, which may be the source of nutrients and energy for prebiotic chemical reactions that could lead to the emergence of life.

Enceladus is the only Ocean World where current geologic activity undoubtedly emits materials from the internal ocean into its exosphere. *Cassini* observed over a hundred jets converging into a plume (Porco et al., 2006), which originates from a set of four rectilinear surface fractures dubbed Tiger Stripes (Spitale & Porco, 2007). Enceladus' plume consists of micron-size particles mostly comprised of water ice that feed Saturn's E ring (Kempf et al., 2010). These particles also contain percent-level NaCl (Postberg et al., 2009; Postberg et al., 2011) and complex organic materials (Postberg et al., 2018). The plume contains volatiles such as ammonia, carbon dioxide, low-mass organics, ^{40}Ar (Waite et al., 2009), and molecular H_2 (Waite et al., 2017). The moderately high pH derived for the ocean (Glein et al., 2015), the plume composition, and the abundant geologic energy from the interior and within the south polar terrain entice the prospect that life may have emerged and still be present on Enceladus (McKay et al., 2008; McKay et al., 2014; McKay et al., 2018).

Europa's surface bears evidence for activity in the recent geologic past and a strong habitability potential. Its surface age is estimated to 60-100 My (Zahnle et al., 2008; Bierhaus et al., 2009). Geochemical modeling of water-rock interactions suggests that Europa's internal ocean may be habitable (Zolotov & Shock, 2001b; Zolotov & Shock, 2001a, 2003; Zolotov & Kargel, 2009). The characterization of possible present-day plume activity at Europa is still an area of active research (Roth et al., 2014; Sparks et al., 2016; Jia et al., 2018; Paganini et al., 2019). The *Europa Clipper* mission (Pappalardo et al., 2015), in development at time of writing, is equipped to detect and analyze such plumes. Until more definitive information is available, it seems reasonable to consider that Europa may emit materials from its internal ocean in a manner akin to Enceladus.

Cassini observations of Enceladus plume particles enabled the determination of their grain size distribution, their trajectories, and their deposition back onto the surface. The mean radius of equivalent-sphere particles determined from imaging is 3.1 ± 0.5 μm (Ingersoll & Ewald, 2011). A particle ejection model was derived from the vertical structure of the plume (Schmidt et al., 2008). The deposition of plume particles can then be computed as a function of particle size, source location, and location on the Enceladus surface (Kempf et al., 2010; Southworth et al., 2019). Particles with radii 0.1 – 5 μm are expected to dominate the plume deposits. The deposition rate averages on order of 1 μm/yr across the entire Enceladus surface, but can be up to 1 mm/yr in locations close to jet sources.

Plumes on Enceladus and perhaps Europa could carry biosignatures, or even microbial life forms, and deposit them on their surface (Porco et al., 2017; Guzman et al., 2019). Other extrusion mechanisms have also been proposed on Europa, such as diapirism (Pappalardo & Barr, 2004). The prospect of finding life, or traces of it, on Europa and Enceladus has motivated the development of mission concepts to explore their surface (Hand, 2017). At time of writing, an Enceladus mission concept is under study to support the upcoming Planetary Science and Astrobiology Decadal Survey for 2023-2032.

Plume deposits are expected to consist of ice particles that form a granular unconsolidated material, which may subsequently evolve over time in a fashion similar to snow on Earth. Snow undergoes a sintering process, in which redistribution of water molecules between grains initiates bonding between grains at their neck, and continues to evolve into a dense material such as in glaciers (Blackford, 2007). However, melting and refreezing processes play an important role in the evolution of snow, making it a relatively poor analog. Sintering of ice particles in planetary environments is the subject of active research. Mass redistribution of ice and growth of the contact regions between grains is anticipated, while a high bulk porosity could be retained over long timescales (Molaro et al., 2019).

The mechanical properties of fine-grained plume deposits under Enceladus and Europa's surface conditions are poorly constrained to date. In this article we present the first laboratory study of the time evolution of the mechanical properties of fine-grained ice particles similar to those of Enceladus' plume at a range of temperatures. We derive the rate of strengthening and its temperature dependence from these measurements, then extrapolate the results to Europa and

Enceladus' surface conditions to estimate and compare the mechanical properties of plume deposit regions on these two bodies.

2. Mechanical resistance of ice plume deposit analogs

Fine-grained (12 μm mean diameter particles) crystalline ice was synthesized by air atomization and deposition in liquid nitrogen. Large samples of unpacked ice particle aggregates (porosity of 51.5 +/- 1.6 %), weighing between 0.66 and 2.14 kg each, were left to sinter in sealed containers under isothermal conditions (193 K, 223 K, 233K, 243 K) for periods of time ranging from a few months up to 14 months, depending on temperature. The mechanical strength of the samples was measured routinely using a custom-built cone penetrometer apparatus. A complete description of materials and methods, and a summary of experiments and samples are presented in Supplementary Information (Text S1, Figures S1-S4, Tables S1-S2).

Every time a cone penetration test was conducted on a sample, we obtained a cone penetration resistance profile as a function of depth within the probed portion of sample. Two example profiles are illustrated in Figure 1 and show extreme end-members of strength profiles obtained. The weakest measurement is from an ice sample just after synthesis (Figure 1-a), and the strongest is from an ice sample that spent 288 days at 223 K (Figure 1-b).

The average resistance of each cone penetration profile was derived as follows. The initial contact of the cone penetrometer with the samples (upper ~ 3 cm) was neglected, since the plastic zone that forms around the cone tip as it passes through the material has not fully developed yet (Rogers, 2006). The bottom 0.5 cm of the strength profiles was also excluded, as we stopped the cone penetrometer ~ 3 cm from the bottom of the sample containers during measurements. The mean value of the strength profile in the remaining mid-section of the samples, between 3 cm and approx. 9 cm depth (3 cm from container bottom), was then taken to be representative of the average strength of the sample in that profile. The error on each average strength measurement was derived from the 1-σ standard deviation around this mean value.

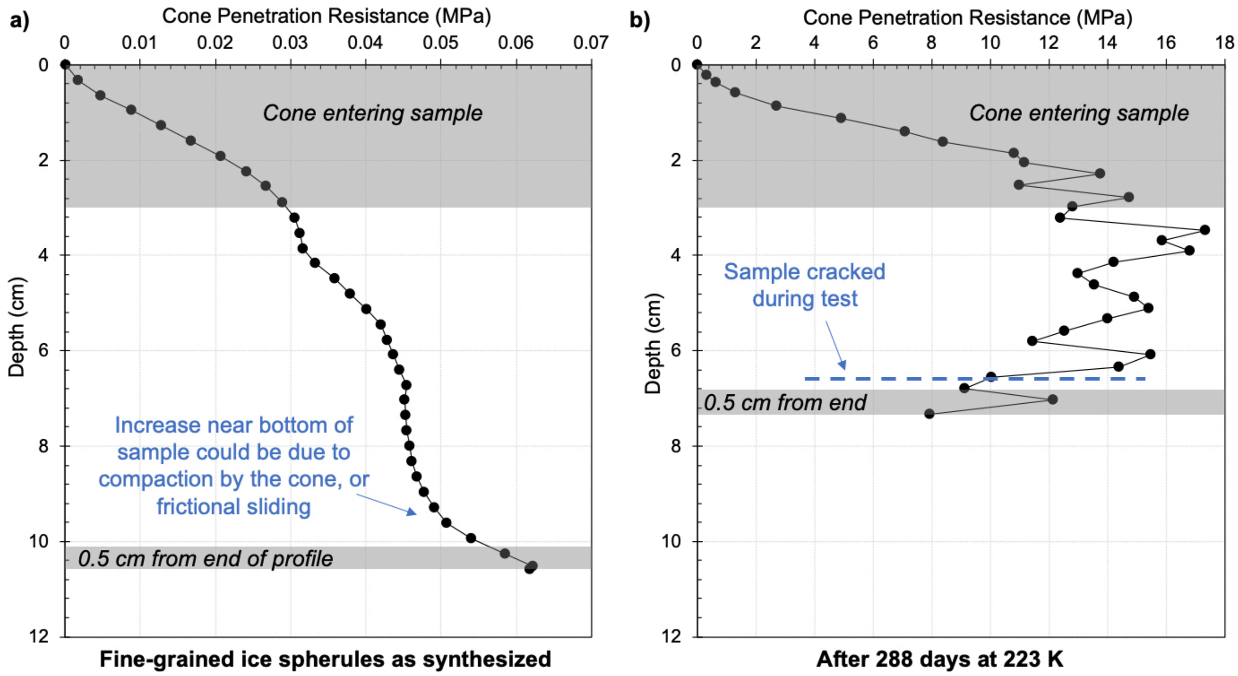

Figure 1. Examples of cone penetration resistance profiles from two end-member situations: *a)* ice just after sample preparation, *b)* ice sintered for 288 days at 223 K. In both profiles, the first 3 cm and the last 0.5 cm in the profiles (which may be within 3 cm from bottom of the container) are not representative of the samples' strength. Note the increase in resistance of more than two orders of magnitude upon sintering over 9.5 months at 223 K.

3. Strength evolution of plume deposit analogs upon sintering

Figure 2-a shows the evolution in average cone penetration resistance of all ice samples. One sample at 223 K exhibited a different strength evolution from the others and was discarded in the analysis (Text S2). At each temperature, strengthening is observed over time and forms seemingly linear trends, which we constrained through a linear regression that included weighting by error bars on individual data points. Temperature has a strong effect on the rate of strengthening: samples held at 193 K only developed a resistance around 2-3 MPa after nearly 400 days, while samples held at 243 K developed a resistance of 7-10 MPa in just 60 days. Table S3 reports the numerical values of fit parameters at each temperature and their 2σ errors. The best-fit parameters yield trend lines that do not encompass the strength of the fresh ice samples, which suggests some early strengthening, perhaps associated to a different process in the evolution of the samples. We have not attempted to further refine fits, because this effect is only obvious at the warmer temperatures, and the dispersion within the dataset is such that more complex fit functions would not have a greater probability of accurately fitting the data.

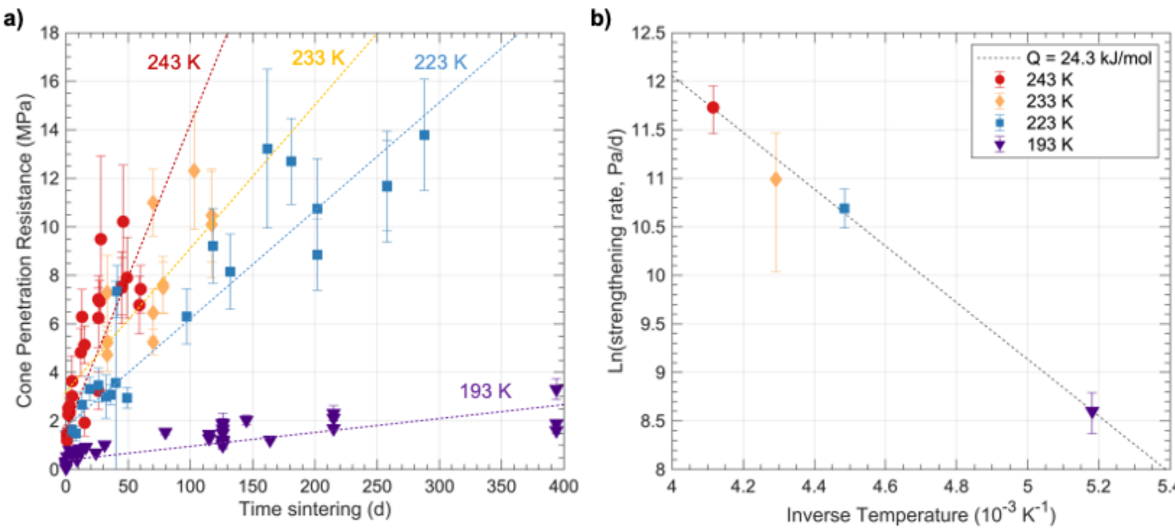

Figure 2. Measured evolution in cone penetration resistance of all samples as a function of time *(a)*, and Arrhenius plot of strengthening rate as a function of inverse temperature *(b)*. Slopes of linear trends derived from measurements at each temperature *(a)* are used to derive the activation energy *(b)* that represents the effect of temperature on these rates, and enables extrapolation to colder temperatures (Section 5).

An Arrhenius plot shows in Figure 2-b the natural logarithm of the rate of strengthening as a function of inverse sample temperature. The error bars correspond to the 95% confidence interval of the strengthening rate at each temperature. The four data points follow a line in this representation, whose slope is by definition -Q/R, where Q is the activation energy of the considered rate as a function of temperature, and R is the ideal gas constant 8.314 J/(mol.K). A linear regression of the dataset, weighted by the standard deviation of the measurements, yields an activation energy Q = 24.3 ± 3.3 kJ/mol (95% confidence interval).

This activation energy is comparable to that of the strength of hydrogen bonds (Suresh & Naik, 2000), as well as to the ~ 23 kJ/mol activation energy of H_2O self-diffusion on the surface of ice grains (Nasello et al., 2007). It is not consistent with the activation energy associated with ice recrystallization (~ 50 kJ/mol), nor with the volume (~ 60 kJ/mol) or vapor (~ 51 kJ/mol) diffusion mechanisms that contribute to the sintering process (Molaro et al., 2019). This suggests that the strengthening of fine-grained ice deposits upon sintering is primarily due to the evolution of a mesoscale network between individual grains, or agglomerates thereof.

4. Implications for mechanical behavior of ice plume deposit analogs

The two cone penetration resistance profiles shown in Figure 1 seem to indicate different kinds of mechanical response during testing between unconsolidated and heavily sintered ice. One kind is exhibited by aggregates of either little or no cohesion amongst grains and is characterized by a very low average cone penetration resistance, that nevertheless increases roughly linearly with depth (Figure 1-a). This is reminiscent of the behavior of dry, polar snow of similar density (McCallum, 2012; McCallum, 2014). The other kind is exhibited by aggregates comprised of grains that, through the temporally and thermally dependent process of sintering, develop significant cohesion amongst themselves and thus possess a much higher collective resistance, around 14 MPa in the example shown in Figure 1-b. This resistance, while oscillating, is more or less independent of depth once the cone has penetrated some distance into the material. The two kinds of mechanical behavior likely originate from different grain-scale interactions.

We examined the strength-depth correlation factor and the relative dispersion within each of the 100 cone penetration profiles obtained, in order to investigate whether the difference in behavior is well represented in our dataset and to constrain the stage of consolidation (cone penetration resistance) at which a transition between deformation regimes may occur. The relative dispersion is the ratio of the standard deviation in cone penetration resistance over the mean cone penetration resistance in each profile. The strength-depth correlation factor κ relates strength S and depth x in each profile, and may indicate depth-strengthening (positive values) or depth-weakening (negative values) behaviors. κ is expressed as follows:

$$\kappa = \frac{\sum_i (S_i - \bar{S})(x_i - \bar{x})}{\sigma_S \sigma_x} \qquad (1)$$

where S_i and x_i indicate the individual measurements of strength and depth along the profile, respectively, $\bar{S}$ and $\bar{x}$ are the mean strength and mean depth of the profile, respectively, and σ_S and σ_x are the standard deviation around the mean strength and mean depth, respectively.

At first sight, the strength-depth correlation factor (Figure 3-a) and the relative dispersion (Figure 3-b) may seem mostly scattered throughout the dataset. However, very high positive correlation factor values (depth-strengthening) are clustered at resistances below 2 MPa. Also, an increasing trend in relative dispersion with resistance is observed. Although the increase in relative dispersion throughout the range of measured cone penetration resistances is smaller than the total dispersion of the dataset (σ = 0.1), the mean relative dispersions at resistances < 1 MPa and > 2 MPa are separated by more than one standard deviation of these two populations (σ ~ 0.05 in both). These observations suggest that a transition between mechanical behaviors could be reflected in the dataset at the low end of measured cone penetration resistance values.

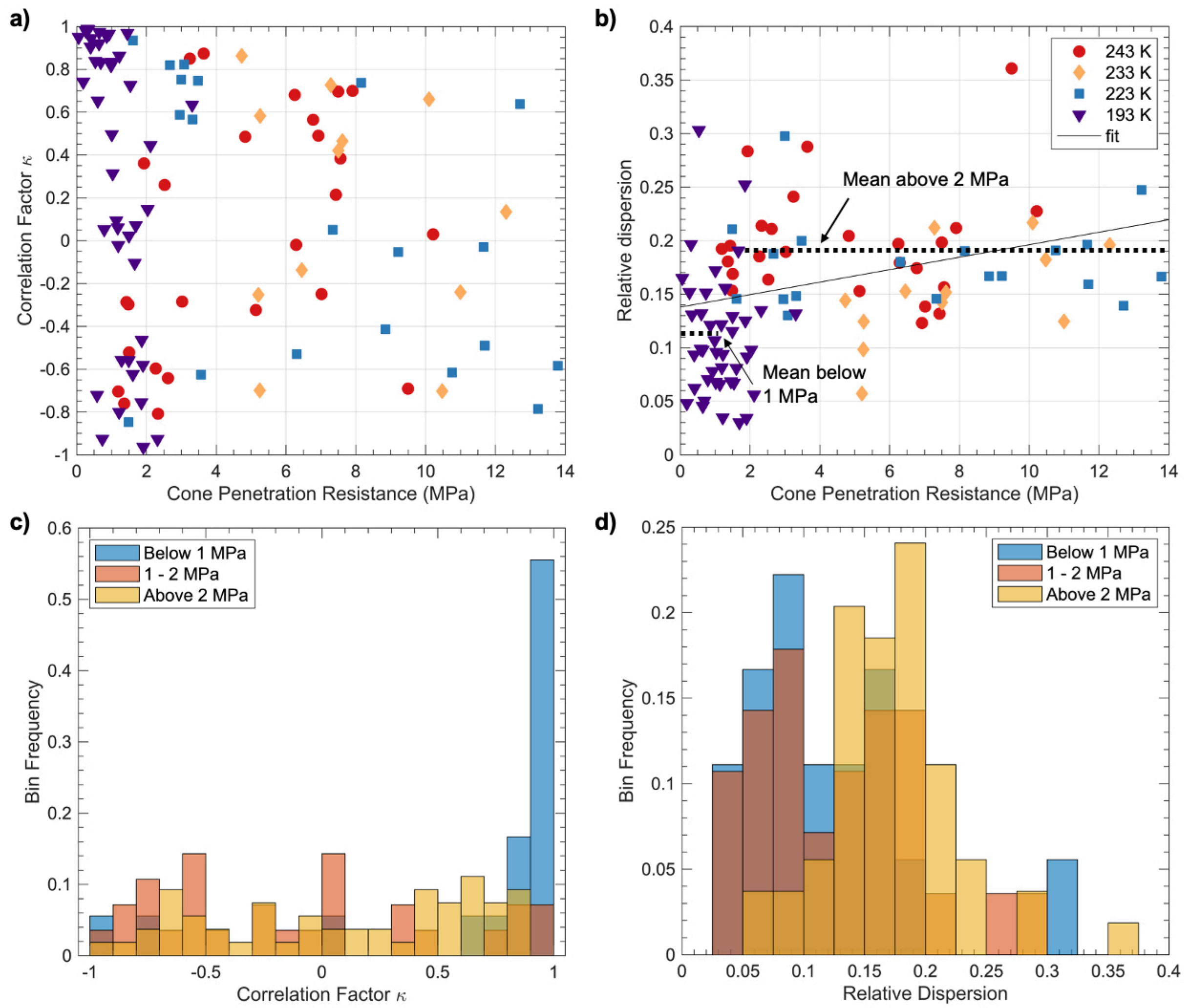

Figure 3. *(a)* Strength-depth correlation factor as a function of cone penetration resistance for all profiles. Color coding follows temperature as in panel *(b)*. *(b)* Relative dispersion (standard deviation over cone penetration resistance) as a function of cone penetration resistance for all profiles; one outlier is not shown. These datasets, along with histograms of the distribution of correlation factor *(c)* and relative dispersion *(d)* within different ranges of cone penetration resistance, suggest a transition between two different mechanical behaviors around 1-2 MPa.

The distribution of strength-depth correlation factor and relative dispersion within three ranges of cone penetration resistance (below 1MPa, 1-2 MPa, above 2 MPa) point to a transition in mechanical behavior around 1-2 MPa in our samples (Figure 3-c and 3-d). For resistance < 1 MPa, the correlation factor indicates a depth-strengthening behavior, and the relative dispersion is dominated by a mode centered around 0.05-0.1, although a second mode is visible. For resistance in the range 1-2 MPa, the depth-strengthening behavior does not dominate anymore, while the relative dispersion shows a decrease in frequency of low-end values and an increase in frequency of the second mode, centered around 0.15-0.2. For resistance > 2 MPa, the correlation factor appears uniformly distributed, while the relative dispersion only exhibits the second mode that is consistent with the mean value of 0.19 above 2 MPa.

The two kinds of mechanical behaviors can be interpreted as follows: response of an unconsolidated aggregate of ice grains below 1 MPa, and brittle compressive failure of a consolidated aggregate above 2 MPa. Below 1 MPa, the linear increase in resistance with depth (Figure 1-a) is consistent with high positive values of the strength-depth correlation factor. This linear increase has been observed in other cone penetration and micropenetrometer measurements conducted in dry, polar snow, where it was attributed to frictional sliding of unconsolidated ice against the steel rod as the cone-rod assembly advanced (McCallum, 2012; McCallum, 2014), and to compaction of the unconsolidated ice ahead of the cone (van Herwijnen, 2013). Above 2 MPa, brittle compressive failure of the cohesive aggregate, in which a rigid network has already developed between grains to the scale of the samples, would explain all findings in that regime: the jerky indentation seen in cone penetration profiles (Figure 1-b), the approximately constant relative dispersion, the absence of strength-depth correlation, and a resistance of overall magnitude comparable to the brittle compressive strength of ice. Future studies investigating the transition between mechanical behaviors may refine this interpretation.

5. Implications for strength of surface plume deposits on Enceladus and Europa

The cone penetration resistance of icy plume deposit analogs increases linearly over time at a given temperature (Section 3). Using the activation energy Q derived from our dataset, the rate of strengthening $r_S(T)$ at a given temperature can be predicted by:

$$\ln r_S = \ln r_0 - \frac{Q}{RT} \qquad (2)$$

where r_0 is the intercept of the rate of strengthening determined from the Arrhenius plot (Figure 2-b).

This Arrhenius expression necessarily assumes that the evolution of the strengthening rate can be reliably extrapolated outside of the temperature range where it was derived from the experimental data (Figure 2). This assumption appears justified to derive at least an upper bound of the resistance of these materials for the following reasons. 1) The surface of Enceladus is dominated by the same hexagonal ice I_h as used in our experiments (Filacchione et al., 2007; Filacchione et al., 2010). 2) The surface of Europa may contain a small fraction of amorphous ice due to irradiation effects, but it appears nevertheless dominated by ice I_h (Hansen & McCord, 2000; Berdis et al., 2020). 3) Low H_2O vapor pressure and airless conditions at the surface of Europa and Enceladus would ease release and escape of H_2O, which suggests that ice could redistribute less efficiently within plume deposits than in our experiments. 4) The effect of temperature on sintering rates strongly dominates over that of grain size (Molaro et al., 2019), such that a one to two order of magnitude difference in the mean grain size between our samples and actual fresh plume deposits on Enceladus and Europa is not anticipated to alter the conclusions of this study.

In Figure 4 we explore how the strengthening rate from the experimental data evolves under the surface conditions of Europa and Enceladus. Approximate temperature ranges at Enceladus are based on *Cassini* data, where South polar terrain mean temperatures can be colder than 50 K, while noontime equatorial temperatures can reach over 80 K (Howett et al., 2010), and temperature at the Tiger Stripes was evaluated to ~ 180 K (Spencer & Nimmo, 2013). Approximate temperature ranges for Europa are based on *Galileo* data (Spencer et al., 1999). The predicted rates of strengthening as a function of temperature for best-fit and $\pm 2\sigma$ Q values from Eq. 2 are shown in Figure 4-a. From this, the cone penetration resistance of icy plume deposits is predicted as a function of temperature and time (Figure 4-b).

It is important to note that our laboratory experiments do not inform whether the strengthening rate eventually decreases and an ultimate cone penetration resistance value may be reached, which would be expected once ice sintering nears completion. The highest resistance recorded in our experiments was 14 MPa, but it was still increasing linearly at the time and no densification had yet occurred. For comparison, the uniaxial unconfined compressive strength of compact water ice at 233 K is around 30 MPa (Petrovic, 2003), and it increases with decreasing temperature up to 60-80 MPa at temperatures 70-130 K (Arakawa & Maeno, 1997; Schulson & Duval, 2009). However, the relationship between cone penetration resistance and unconfined compressive strength is not trivial and depends strongly on materials microstructure, test characteristics, and modes of failure. In the case of poorly consolidated snow (< 1 MPa), cone penetration resistance and unconfined compressive strength have very comparable values (McCallum, 2012). Further investigating this would require a dedicated study and goes beyond the scope of this article. For order of magnitude, we estimate that a cone penetration resistance greater than 10 MPa corresponds to a heavily sintered (albeit still porous) material, and predicted values higher than 100 MPa are not shown in Figure 4-b.

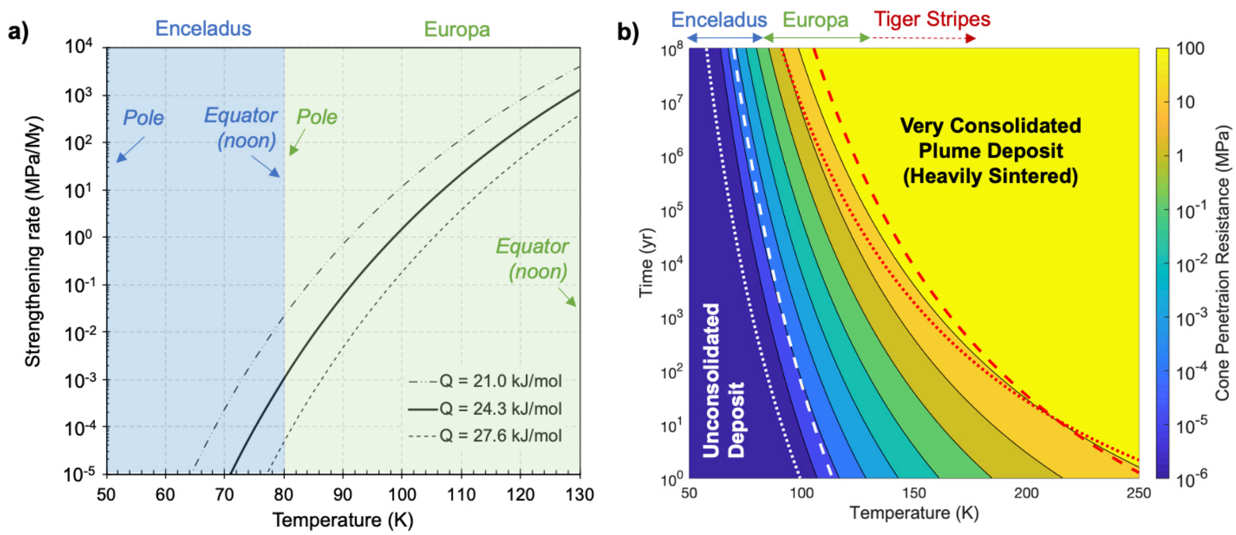

Figure 4. *(a)* Predicted strengthening rate of icy plume deposits as a function of temperature, for the best-fit activation energy, and for values +2σ and -2σ from it. Representative temperature ranges at equilibrium for polar and equatorial midday conditions on Enceladus and Europa are illustrated for comparison. *(b)* Predicted cone penetration resistance of icy plume deposits as a function of temperature and sintering time. Black contours are for the best-fit activation energy value. Dashed and dotted contours illustrate the effect of the uncertainty on activation energy of +2σ and -2σ, respectively. For legibility, these contours are only shown for the 10^{-5} (white) and 100 MPa (red) cone penetration resistance levels.

Under typical Enceladus surface conditions, little to no strengthening is expected for plume deposits. In the South polar region, it would take at least the age of the Solar system for the deposits to develop a resistance on order of 1 MPa (Figure 4-a). Under Enceladus equatorial noontime temperatures, plume deposits would still take about 100 My to reach 1 MPa cone penetration resistance. For comparison, our laboratory samples of 1 MPa cone penetration resistance are poorly consolidated, and friable by hand. Thus, plume deposits in these areas are anticipated to remain poorly consolidated and relatively easy to sample.

Close to the Tiger Stripes, where temperatures up to 180 K have been estimated (Spencer & Nimmo, 2013), plume deposit materials would develop a cone penetration resistance around

10 MPa in ~ 15 years. For comparison, our laboratory samples with a cone penetration resistance on order of 10 MPa are very consolidated. Cracks and faulting planes develop and propagate across the entire samples on failure. Excavating and acquiring samples of such materials would require tools able to break the materials and generate tailings, such as rasps or drills.

However, these regions close to the Tiger Stripes are also areas where the deposition of new plume deposits would be most intense, on order of 0.01 to 1 mm/yr (Kempf et al., 2010; Southworth et al., 2019). There would be competition between strengthening of existing plume deposits and covering by new fresh and loose particles, therefore the spatial distribution in deposition rate across the surface could be an important factor for selecting sampling sites. Depending on the local deposition rate and thermal environment, one may seek plume deposit areas that are fresh enough to remain poorly consolidated over the first few centimeters.

Europa is an intermediate situation between Enceladus' nominal surface conditions and its hot spots at the Tiger Stripes. Europa's surface temperature ranges from around 80 K in the nighttime up to > 130 K for noon time equatorial temperatures (Spencer et al., 1999), and its annual mean is around 100 K. The expected cone penetration resistance of plume deposits can vary from that of unconsolidated or poorly consolidated ice grains in fresh deposits and/or in the winter polar regions, to that of very consolidated materials in geologically old deposits and/or the equatorial regions. The latter would require a sampling approach that includes means to break up surface materials, collect the tailings and then transfer them for analysis. Such an approach is being considered for the potential Europa lander mission concept, currently in formulation (Hand, 2017).

6. Conclusions

This study presents the first experimental investigation of the impact of sintering on the strength of bulk ice plume deposit analog samples relevant to Enceladus and Europa. Ice plume deposit analogs were left to sinter under isothermal conditions and at water vapor saturation pressure for up to 14 months. Cone penetration resistance measurements conducted over the course of the experiments showed a linear increase in strength with respect to time at all temperatures. A transition between two mechanical behavior regimes occurs around 1-2 MPa cone penetration resistance. The temperature dependence of the rate of strengthening follows an Arrhenius relationship and yields an activation energy of 24.3 ± 3.3 kJ/mol. This value is consistent with a process dominated by self-diffusion of H_2O molecules on the surface of ice grains. Extrapolation to the surface conditions of Enceladus and Europa suggests that little strengthening would occur on Enceladus, except in hot spot regions that do not experience subsequent deposition of fresh plume particles, while substantial strengthening may occur on Europa over geologic timescales.

At a time where the surface and subsurface exploration of Ocean Worlds is a high priority of the planetary science community, these results have implications for the design of landing and sampling systems for future landed missions to Enceladus and Europa. They also highlight the importance of assessing and anticipating the surface properties via laboratory studies and modeling to support the selection of candidate landing and sampling sites.

Acknowledgments

Part of this work has been conducted at the Jet Propulsion Laboratory, California Institute of Technology, under contract to the National Aeronautics and Space Administration. The authors are grateful to Adrian McCallum and an anonymous reviewer for providing comments that helped improve this manuscript. The authors would like to acknowledge A. Mahjoub and student interns who assisted in the development of the sample preparation system and characterization procedures (D. Naiman, S. Dalessi), of the upright cone penetrometer apparatus (E. Carpenter), and in conducting early measurements for this study (E. Phelps). All authors have no conflicts of interest. Support from the JPL Research and Technology Development Program is gratefully acknowledged. Tabular data supporting the analysis and conclusions of this article, and necessary to reproduce the figures shown in the article, are found at *data.caltech.edu/records/1431* (DOI: 10.22002/D1.1431). Government sponsorship acknowledged.

References

Anderson, J. D., Schubert, G., Jacobson, R. A., Lau, E. L., Moore, W. B., & Sjogren, W. L. (1998). Europa's Differentiated Internal Structure: Inferences from Four Galileo Encounters. *Science, 281*, 2019.

Arakawa, M., & Maeno, N. (1997). Mechanical strength of polycrystalline ice under uniaxial compression. *Cold regions science and technology, 26*(3), 215-229.

Berdis, J. R., Gudipati, M. S., Murphy, J. R., & Chanover, N. J. (2020). Europa's surface water ice crystallinity: Discrepancy between observations and thermophysical and particle flux modeling. *Icarus, 341*, 113660.

Bierhaus, E. B., Zahnle, K., Chapman, C. R., Pappalardo, R., McKinnon, W., & Khurana, K. (2009). Europa's crater distributions and surface ages. *Europa*, 161-180.

Blackford, J. R. (2007). TOPICAL REVIEW: Sintering and microstructure of ice: a review. *Journal of Physics D Applied Physics, 40*, R355.

Carey, E. M., Peters, G. H., Choukroun, M., Chu, L., Carpenter, E., Cohen, B., Panossian, L., Zhou, Y. M., Sarkissian, A., Moreland, S., Shiraishi, L. R., Backes, P., Zacny, K., Green, J. R., & Raymond, C. (2017). Development and characteristics of Mechanical Porous Ambient Comet Simulants as comet surface analogs. *Planetary and Space Science, 147*, 6-13.

Choukroun, M., Barmatz, M., & Castillo-Rogez, J. (2011). Understanding Evolution of Icy Satellites through Cryogenic Light Microscopy and Raman Studies. *Microscopy and Analysis-UK*(144), 5.

Filacchione, G., Capaccioni, F., Clark, R. N., Cuzzi, J. N., Cruikshank, D. P., Coradini, A., Cerroni, P., Nicholson, P. D., McCord, T. B., Brown, R. H., Buratti, B. J., Tosi, F., Nelson, R. M., Jaumann, R., & Stephan, K. (2010). Saturn's icy satellites investigated by Cassini-VIMS. II. Results at the end of nominal mission. *Icarus, 206*, 507.

Filacchione, G., Capaccioni, F., McCord, T. B., Coradini, A., Cerroni, P., Bellucci, G., Tosi, F., D'Aversa, E., Formisano, V., Brown, R. H., Baines, K. H., Bibring, J. P., Buratti, B. J., Clark, R. N., Combes, M., Cruikshank, D. P., Drossart, P., Jaumann, R., Langevin, Y., Matson, D. L., Mennella, V., Nelson, R. M., Nicholson, P. D., Sicardy, B., Sotin, C., Hansen, G., Hibbitts, K., Showalter, M., & Newman, S. (2007). Saturn's icy satellites investigated by Cassini-VIMS. I. Full-disk properties: 350 5100 nm reflectance spectra and phase curves. *Icarus, 186*, 259.

Glein, C. R., Baross, J. A., & Waite Jr, J. H. (2015). The pH of Enceladus' ocean. *Geochimica Et Cosmochimica Acta, 162*, 202-219.

Glein, C. R., Zolotov, M. Y., & Shock, E. L. (2008). The oxidation state of hydrothermal systems on early Enceladus. *Icarus, 197*(1), 157-163.

Guzman, M., Lorenz, R., Hurley, D., Farrell, W., Spencer, J., Hansen, C., Hurford, T., Ibea, J., Carlson, P., & McKay, C. P. (2019). Collecting amino acids in the Enceladus plume. *International Journal of Astrobiology, 18*(1), 47-59.

Hand, K. P. (2017). *Report of the Europa Lander science definition team*: National Aeronautics and Space Administration.

Hansen, G. B., & McCord, T. B. (2000). *Amorphous and Crystalline Ice on the Galilean Satellites: A Balance Between Thermal and Radiolytic Processes*. Paper presented at the Lunar and Planetary Science Conference. https://ui.adsabs.harvard.edu/abs/2000LPI....31.1630H

Howett, C., Spencer, J., Pearl, J., & Segura, M. (2010). Thermal inertia and bolometric Bond albedo values for Mimas, Enceladus, Tethys, Dione, Rhea and Iapetus as derived from Cassini/CIRS measurements. *Icarus, 206*(2), 573-593.

Iess, L., Stevenson, D., Parisi, M., Hemingway, D., Jacobson, R., Lunine, J., Nimmo, F., Armstrong, J., Asmar, S., & Ducci, M. (2014). The gravity field and interior structure of Enceladus. *Science, 344*(6179), 78-80.

Ingersoll, A. P., & Ewald, S. P. (2011). Total particulate mass in Enceladus plumes and mass of Saturn's E ring inferred from Cassini ISS images. *Icarus, 216*(2), 492-506.

Jia, X., Kivelson, M. G., Khurana, K. K., & Kurth, W. S. (2018). Evidence of a plume on Europa from Galileo magnetic and plasma wave signatures. *Nature astronomy, 2*, 459-464.

Kempf, S., Beckmann, U., & Schmidt, J. (2010). How the Enceladus dust plume feeds Saturn's E ring. *Icarus, 206*(2), 446-457.

McCallum, A. (2014). A brief introduction to cone penetration testing (CPT) in frozen geomaterials. *Annals of Glaciology, 55*(68), 7-14.

McCallum, A. B. (2012). *Cone penetration testing in polar snow.* University of Cambridge, McKay, C., Davila, A., Glein, C., Hand, K., & Stockton, A. (2018). Enceladus astrobiology, habitability, and the origin of life. *Enceladus and the Icy Moons of Saturn; Schenk, PM, Clark, RN, Howett, CJA, Verbiscer, AJ, Waite, JH, Eds*, 437-452.

McKay, C. P., Anbar, A. D., Porco, C., & Tsou, P. (2014). Follow the plume: the habitability of Enceladus. *Astrobiology, 14*(4), 352-355.

McKay, C. P., Porco, C. C., Altheide, T., Davis, W. L., & Kral, T. A. (2008). The possible origin and persistence of life on Enceladus and detection of biomarkers in the plume. *Astrobiology, 8*(5), 909-919.

Molaro, J. L., Choukroun, M., Phillips, C. B., Phelps, E. S., Hodyss, R., Mitchell, K. L., Lora, J. M., & Meirion-Griffith, G. (2019). The Microstructural Evolution of Water Ice in the Solar System Through Sintering. *Journal of Geophysical Research (Planets), 124*, 243-277.

Nasello, O., de Juarez, S. N., & Di Prinzio, C. (2007). Measurement of self-diffusion on ice surface. *Scripta materialia, 56*(12), 1071-1073.

Nimmo, F., & Pappalardo, R. (2016). Ocean worlds in the outer solar system. *Journal of Geophysical Research: Planets, 121*(8), 1378-1399.

Paganini, L., Villanueva, G. L., Roth, L., Mandell, A., Hurford, T., Retherford, K. D., & Mumma, M. J. (2019). A measurement of water vapour amid a largely quiescent environment on Europa. *Nature astronomy*, 1-7.

Pappalardo, R. T., Senske, D. A., Prockter, L. M., Paczkowski, B., Vance, S., Goldstein, B., Magner, T., & Cooke, B. (2015). *Science and Reconnaissance from the Europa Clipper Mission Concept: Exploring Europa's Habitability*. Paper presented at the Lunar and Planetary Science Conference. https://ui.adsabs.harvard.edu/abs/2015LPI....46.2673P

Pappalardo, R. T., & Barr, A. C. (2004). The origin of domes on Europa: The role of thermally induced compositional diapirism. *Geophysical Research Letters, 31*(1).

Petrovic, J. J. (2003). Review Mechanical properties of ice and snow. *Journal of Materials Science, 38*(1), 1-6.

Porco, C. C., Dones, L., & Mitchell, C. (2017). Could it be snowing microbes on Enceladus? Assessing conditions in its plume and implications for future missions. *Astrobiology, 17*(9), 876-901.

Porco, C. C., Helfenstein, P., Thomas, P., Ingersoll, A., Wisdom, J., West, R., Neukum, G., Denk, T., Wagner, R., & Roatsch, T. (2006). Cassini observes the active south pole of Enceladus. *Science, 311*(5766), 1393-1401.

Postberg, F., Khawaja, N., Abel, B., Choblet, G., Glein, C. R., Gudipati, M. S., Henderson, B. L., Hsu, H.-W., Kempf, S., & Klenner, F. (2018). Macromolecular organic compounds from the depths of Enceladus. *Nature, 558*(7711), 564-568.

Postberg, F., Schmidt, J., Hillier, J., Kempf, S., & Srama, R. (2011). A salt-water reservoir as the source of a compositionally stratified plume on Enceladus. *Nature, 474*(7353), 620-622.

Postberg, F., Kempf, S., Schmidt, J., Brilliantov, N., Beinsen, A., Abel, B., Buck, U., & Srama, R. (2009). Sodium salts in E-ring ice grains from an ocean below the surface of Enceladus. *Nature, 459*(7250), 1098-1101.

Rogers, J. D. (2006). Subsurface exploration using the standard penetration test and the cone penetrometer test. *Environmental and Engineering Geoscience, 12*(2), 161-179.

Roth, L., Saur, J., Retherford, K. D., Strobel, D. F., Feldman, P. D., McGrath, M. A., & Nimmo, F. (2014). Transient Water Vapor at Europa's South Pole. *Science, 343*, 171-174.

Schmidt, J., Brilliantov, N., Spahn, F., & Kempf, S. (2008). Slow dust in Enceladus' plume from condensation and wall collisions in tiger stripe fractures. *Nature, 451*, 685.

Schubert, G., Anderson, J. D., Travis, B. J., & Palguta, J. (2007). Enceladus: Present internal structure and differentiation by early and long-term radiogenic heating. *Icarus, 188*(2), 345-355.

Schulson, E. M., & Duval, P. (2009). *Creep and fracture of ice*: Cambridge University Press.

Sekine, Y., Shibuya, T., Postberg, F., Hsu, H.-W., Suzuki, K., Masaki, Y., Kuwatani, T., Mori, M., Hong, P. K., & Yoshizaki, M. (2015). High-temperature water–rock interactions and hydrothermal environments in the chondrite-like core of Enceladus. *Nature Communications, 6*(1), 1-8.

Sohl, F., Choukroun, M., Kargel, J., Kimura, J., Pappalardo, R., Vance, S., & Zolotov, M. (2010). Subsurface Water Oceans on Icy Satellites: Chemical Composition and Exchange Processes. *Space Science Reviews, 153*(1-4), 485-510.

Sotin, C., & Tobie, G. (2004). Internal structure and dynamics of the large icy satellites. *Comptes Rendus Physique, 5*(7), 769-780.

Southworth, B. S., Kempf, S., & Spitale, J. (2019). Surface deposition of the Enceladus plume and the zenith angle of emissions. *Icarus, 319*, 33.

Sparks, W. B., Hand, K. P., McGrath, M. A., Bergeron, E., Cracraft, M., & Deustua, S. E. (2016). Probing for Evidence of Plumes on Europa with HST/STIS. *The Astrophysical Journal, 829*.

Spencer, J. R., & Nimmo, F. (2013). Enceladus: An active ice world in the Saturn system. *Annual Review of Earth and Planetary Sciences, 41*, 693-717.
Spencer, J. R., Tamppari, L. K., Martin, T. Z., & Travis, L. D. (1999). Temperatures on Europa from Galileo Photopolarimeter-Radiometer: Nighttime Thermal Anomalies. *Science, 284*, 1514.
Spitale, J. N., & Porco, C. C. (2007). Association of the jets of Enceladus with the warmest regions on its south-polar fractures. *Nature, 449*(7163), 695-697.
Suresh, S., & Naik, V. (2000). Hydrogen bond thermodynamic properties of water from dielectric constant data. *The Journal of Chemical Physics, 113*(21), 9727-9732.
van Herwijnen, A. (2013). Experimental analysis of snow micropenetrometer (SMP) cone penetration in homogeneous snow layers. *Canadian geotechnical journal, 50*(10), 1044-1054.
Waite, J. H., Glein, C. R., Perryman, R. S., Teolis, B. D., Magee, B. A., Miller, G., Grimes, J., Perry, M. E., Miller, K. E., & Bouquet, A. (2017). Cassini finds molecular hydrogen in the Enceladus plume: evidence for hydrothermal processes. *Science, 356*(6334), 155-159.
Waite, J. H., Lewis, W., Magee, B., Lunine, J., McKinnon, W., Glein, C., Mousis, O., Young, D., Brockwell, T., & Westlake, J. (2009). Liquid water on Enceladus from observations of ammonia and 40 Ar in the plume. *Nature, 460*(7254), 487.
Zahnle, K., Alvarellos, J. L., Dobrovolskis, A., & Hamill, P. (2008). Secondary and sesquinary craters on Europa. *Icarus, 194*, 660-674.
Zolotov, M. Y., & Kargel, J. S. (2009). On the Chemical Composition of Europa's Icy Shell, Ocean, and Underlying Rocks. In *Europa* (pp. 431).
Zolotov, M. Y., & Shock, E. L. (2003). Energy for biologic sulfate reduction in a hydrothermally formed ocean on Europa. *Journal of Geophysical Research (Planets), 108*.
Zolotov, M. Y., & Shock, E. L. (2001a). Composition and stability of salts on the surface of Europa and their oceanic origin. *Journal of Geophysical Research, 106*, 32815-32828.
Zolotov, M. Y., & Shock, E. L. (2001b). *A hydrothermal origin for the sulfate-rich ocean of Europa.* Paper presented at the Lunar and Planetary Science Conference.